Available online at www.sciencedirect.com
ScienceDirect
Advances in Space Research 39 (2007) 224–229
ADVANCES IN SPACE RESEARCH (a COSPAR publication)
www.elsevier.com/locate/asr

Precision electrostatic suspension system for the Gravity Probe B relativity mission's science gyroscopes

W.J. Bencze *, M.E. Eglington, R.W. Brumley, S. Buchman

HEPL Gravity Probe B, Stanford University, Stanford, CA 94305, USA

Received 30 November 2002; accepted 14 September 2006

Abstract

Presented here is a hybrid digital/analog electrostatic suspension control system for the NASA/Stanford University Gravity Probe B Relativity Mission's science gyroscopes. An adaptive LQE algorithm, called Authority-on-Demand (AOD), has been developed to meet the high dynamic range requirements for mission's electrostatic suspension, while minimizing suspension induced torques on the rotor. AOD is novel because it uses plant state estimates, rather than plant parameter estimates, as inputs for adaptation. In addition minimizing disturbance torques on the gyroscope, this suspension system can also maximize and control disturbances torques to perform a post spin-up alignment of the gyroscope spin axes. A backup all-analog proportional-derivative (PD) controller subsystem is provided to maintain control of the rotor in the event of computer faults/radiation induced upsets. A precision mechanical simulation of the gyroscope's capacitive interface and dynamic response is used to verify performance of the overall system.
© 2006 COSPAR. Published by Elsevier Ltd. All rights reserved.

Keywords: Inertial sensor; Electrostatic suspension; Gyroscope; General relativity; Adaptive control

1. Introduction

The Gravity Probe B Relativity Experiment (GP-B) is a joint NASA/Stanford University orbiting astrophysics experiment, now under development, to test two predictions of Einstein's theory of General Relativity: the *geodetic* and *frame-dragging* effects, the second of which has never been experimentally observed. The relativistic sensors for this experiment are four identical, ultra-precise mechanical gyroscopes carefully isolated from nearly all sources of Newtonian torques. The uncompensated drift rate of these gyroscopes is expected to be less than 0.3 marc-sec/year (1.7×10^{-12} rad/h), about a factor of 10^6 times better than the finest terrestrial navigational gyroscopes. General Relativity predicts that, though isolated from external torques, the spin axes of these gyroscopes will precess with respect to a distant inertial reference frame at a rate of 6.6″/year for the geodetic effect, and 41 marc-sec/year due to frame-dragging in the planned polar, circular orbit at an altitude of 642 km (see Fig. 1). This experiment is designed to measure these effects to an accuracy of 0.5 marc-sec (2.4×10^{-9} rad) (Turneaure, 1996).

Described herein is the design of the gyroscope system and the physical relationships that give rise to the forces and torques on the gyroscope rotor. The overall architecture of the suspension control system is detailed, including both the primary DSP-based suspension algorithm, Authority-on-demand (AOD), and the analog backup system used in the event of computer faults. Briefly described is a scheme where the suspension system uses residual suspension torques in a coordinated way to initially align the spin axis of the rotor to a well-characterized guide star. Finally, a novel testing scheme is described in which the on-orbit performance of the system can be verified in fine detail.

Though this technology has been specifically designed for the Gravity Probe B mission, it readily extensible to other related space-born inertial reference platforms, such as NASA's Space Technology 7 (ST7) gravitational

* Corresponding author.
E-mail address: bencze@relgyro.stanford.edu (W.J. Bencze).

0273-1177/$30 © 2006 COSPAR. Published by Elsevier Ltd. All rights reserved.
doi:10.1016/j.asr.2006.09.020

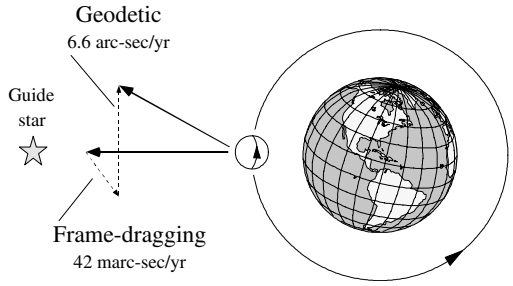

Fig. 1. The two relativistic precessions: geodetic and frame-dragging.

reference sensor initiative and the STEP and LISA projects (Cramer, 2003).

2. The gyroscope

Each gyroscope consists of a 38 mm diameter, 63.5 g, fused quartz sphere coated with a thin layer of niobium metal, a low-temperature superconductor, that is spherical to one part in 10^6 (≈20 nm). It is suspended electrostatically in a spherical cavity via voltages provided through six dish-shaped electrodes located on the housing wall arranged in opposing pairs along three orthogonal axes. The gyroscope is spun up to 5000 rpm (83 Hz) via a tangential gas jet which flows in a channel in the housing (see Fig. 2). To activate the superconducting coating, the gyroscope is cooled to ~2.0 K in a superfluid liquid helium dewar.

The gyroscope's spin axis direction is sensed from measurements of the rotor's London Moment, a dipole magnetic field created by a spinning superconductor whose axis is perfectly aligned with the rotor's instantaneous spin axis. A superconducting pickup loop on the parting plane of the housing couples this magnetic field into a Superconducting Quantum Interference Device (SQUID), a highly sensitive magnetometer, for measurement (Wellstood, 1984) from these measurements over multiple satellite roll periods, the direction of the gyroscope spin axis can be determined with respect to both local inertial and spacecraft-fixed axes.

Fig. 2. Photograph of GP-B gyroscope: rotor and housing. Spin-up channel and 6 dish-like electrodes are clearly seen.

3. Suspension forces and torques

The forces and torques on the gyroscope rotor can be found by considering the change in stored energy in the six capacitors formed by the six electrodes and rotor surface. The capacitance can be described to high accuracy using a parallel plate capacitance model; for one of the six electrodes, i :

$$C_i \approx \int\int \frac{\epsilon_0}{\mathrm{d}(\theta,\phi)}\,\mathrm{d}A = \int\int_{\Omega_i} \frac{\epsilon_0 r_0^2}{\mathrm{d}(\theta,\phi)}\,\mathrm{d}\Omega \tag{1}$$

where $\mathrm{d}(\theta,\phi) = R_0 - r\ (\theta,\ \phi)$ the housing/rotor gap, R_0 the housing radius, and Ω_i is the area under an electrode.

Forces and torques are computed by finding virtual work associated with virtual changes in position and orientation of the rotor (Smythe, 1968):

$$U = \frac{1}{2}\mathrm{C}\mathrm{V}^2 \tag{2}$$

$$\mathbf{F} = -\left.\frac{\partial U}{\partial \mathrm{p}}\right|_{V_{\mathrm{const.}}} \qquad \boldsymbol{\tau} = -\left.\frac{\partial U}{\partial \boldsymbol{\psi}}\right|_{V_{\mathrm{const.}}} \tag{3}$$

Here, U is the electrical energy stored in the capacitor, p is the rotor position vector in the housing, and $\boldsymbol{\psi}$ is an axis of rotation. The voltage on the electrode is held to a desired value by the suspension system drive electronics. The near spherical shape of the rotor suggests that most of the electrostatic *force* on the rotor will be radial. Applying Eq. (3) to the capacitance expression in Eq. (1) the following relation is found for the force due to a displacement along an electrode axis, n, ($n \in \{x, y, z\}$):

$$F_n = K_f\left[\frac{(V_{n+} - V_{\mathrm{r}})^2}{(d_0 - n)^2} - \frac{(V_{n-} - V_{\mathrm{r}})^2}{(d_0 + n)^2}\right] \tag{4}$$

here, the effects of differential displacements from two opposite electrodes ($n+$ and $n-$) are summed to give the net force. A_{e} is the electrode area, n is rotor position relative to the center of the housing along the n-axis, V_{r} is the rotor potential. $K_f = \epsilon_0 A_{\mathrm{e}}/2$. To first order, this force relationship is decoupled from the other two axes. These expressions are nonlinear both in applied voltage and gyroscope position; the equilibrium point is also unstable for constant electrode voltages.

The rotor is insulated by vacuum from other conductors in the housing cavity, thus, its electrostatic potential, V_{r}, becomes a function of the six electrode voltages and six electrode/rotor capacitances. From Eq. (4), it is clear that V_{r} must be controlled in order to generate predictable forces on the rotor, therefore, it is necessary to constrain the six electrode control voltages such that V_{r} is constant (for convenience, $V_{\mathrm{r}} = 0$). This constraint must be taken into account during the calculation of the electrode voltages.

For a desired set of suspension forces, F_x, F_y, and F_z, the voltages are chosen for each electrode axis, n, via the following scheme:

$$V_{n+} = \left[E_{pn} + \frac{u_n}{4K_f E_{pn}}\right](d_0 - \hat{n}) \tag{5}$$

$$V_{n-} = \left[E_{pn} - \frac{u_n}{4K_f E_{pn}}\right](d_0 + \hat{n}) \tag{6}$$

The first term in these equations (in square brackets) inverts the voltage-to-force nonlinearity, while the second inverts position nonlinearity. E_{pn} is an *electric field intensity preload* to be chosen for each axis, u_n is the desired force along the axis, $\hat{n}$ is the measured (or estimated) gyroscope position. When the above are combined with Eq. (4), the net force relation becomes $F_n = u_n$.

The electric field preloads still must be chosen. For a rotor centered in the housing, the six electrode/rotor capacitances are of equal magnitude, and a simple application of Kirchoff's law will show that

$$V_r = 0 \Rightarrow E_{px} + E_{py} + E_{pz} = 0 \tag{7}$$

Here, two of the three electric field preloads must be chosen in order to compute voltages. These choices represent two degrees of freedom in the force equations such that changes in the suspension voltage set resulting from choices of E_{pn} lie in the force null space; changes in voltages consistent with Eq. (7) do not change the suspension force on the rotor. The E_{pn} can be chosen to optimize some cost function of interest; during the mission, the choice changes from *torque maximization* during the period when the spin axis is being aligned to the guide start, to *torque minimization* for nominal science data gathering.

4. Suspension system design

To meet the overall objectives set for the GP-B mission, the forces that the suspension system must present to the gyroscope span a huge dynamic range – eight orders of magnitude – and the system must compensate for a diverse set of disturbances during the various phases of the mission. It is unfeasible to span this space with a fixed control scheme. Thus, a multi-level scheme has been developed to address the pertinent requirements in each of three control modes: (1) science mission, (2) spin-up and alignment, and (3) ground test. Fig. 3 presents a diagram of the suspension controller set and the specific forces and electrode voltages required in by the various modes.

The position of the rotor is measured with three capacitance bridges, one per axis, via a 40 mVpp, 34 kHz sinusoidal sense signal superimposed onto the drive electrodes. This bridge has an operational noise floor of 0.1 nm/$\sqrt{\text{Hz}}$, sufficient resolution to allow the control system to meet the rotor centering requirements for the mission. The magnitude and frequency of the sense signal was chosen so to be compatible with the SQUID magnetometers used to measure the orientation of the rotor's spin axis.

The design is partitioned into two physical enclosures, one forward "analog" section, and one aft "digital" section. The forward section primarily houses the precision analog electronics suite needed by the suspension system

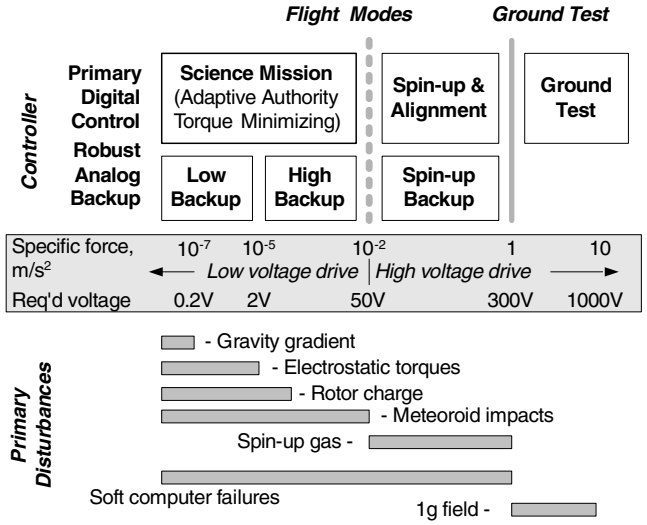

Fig. 3. Suspension controllers and regions of operation (accelerations and voltages).

and also contains a bank of 16-bit A/D and D/A converters to translate the analog drive and position sense signals to their digital equivalents for use in by the aft-mounted computer. Extensive internal shielding is employed to minimize the propagation of high-frequency digital noise to the sensitive analog electronics set. Thermal stability of the analog electronics is of prime concern, especially in a space environment. The required stability is achieved through a passive, multi-layer insulation scheme which will hold the electronics to within 5 mK at the critical roll period of the spacecraft (1–3 min), with an annual excursion of 10 K from the mean temperature of 300 K.

At the heart of the aft digital enclosure is a British Aerospace RAD6000-based CPU which acts as a DSP for control calculations, as well as a system monitoring and communication conduit to the main spacecraft computer. Power is generated for the system via a very low noise DC-to-DC converter system in its own enclosure mounted to the aft box. It generates a warm-redundant set of analog and digital supply voltages for the forward unit, a non-redundant set of voltages for the aft, and a survival heater power for cold periods on orbit. The forward unit supply voltages are further filtered and regulated within the forward enclosure to ensure that conducted EMI is minimized.

4.1. Authority-on-demand control

An adaptive LQE algorithm, called Authority-on-Demand (AOD), has been developed to meet the high dynamic range requirements for mission's electrostatic suspension (Eglington, 2000). The AOD architecture is novel because it uses plant state estimates, rather than plant parameter estimates, as inputs for adaptation. During operation, this allows the algorithm to dynamically increase its control authority (bandwidth) to the level needed to respond to

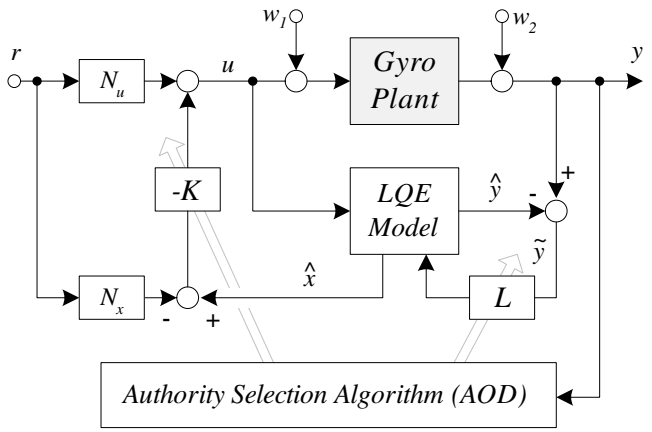

Fig. 4. Block diagram of AOD concept showing disturbance dependent adaptive blocks (L and K).

large impulsive disturbances while continuously minimizing control authority during nominal operation and thus minimizing residual torques on the rotor. The net result of this scheme is that the control system performs like a high-bandwidth and high-authority controller with respect to disturbances, but acts like a low-torque, low-authority control system with respect to gyroscope disturbance torques. Fig. 4 depicts the basic structure of the AOD controller; the authority selection algorithm computes new LQE gains, L, and state feedback gains, K, to stiffen the control response as the magnitude of the disturbance increases. Fig. 5 shows a set of responses to micrometeoroid strikes (steps at w_2 in Fig. 4). It is important to note that the magnitude of the excursion is roughly constant regardless of the magnitudes of the disturbance (the oscillations seen is a spacecraft structure resonance, not a sign of controller instability).

The digital spin-up and ground test controllers are also implemented in the suspension processor, but are of a less sophisticated design. The primary character of both of these modes is that they must handle a quasi-DC disturbance as part of their nominal operation. The spin-up controller is required to hold the rotor near the spin-up channel in the presence of a specific force on the order

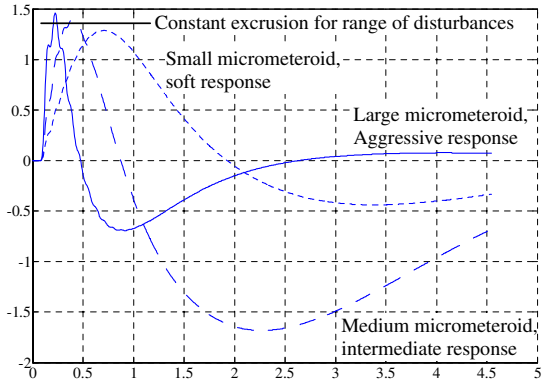

Fig. 5. AOD provides nearly constant excursion control for 10× range of disturbances.

of 1 m/s^2 during the time spin-up gas is flowing. In a similar way, the ground test controller must suspend the gyroscope against the 9.81 m/s^2 acceleration of the Earth's gravitational field. These high specific forces require high suspension voltages, and thus, a spin-up/ground test high voltage amplifier is needed to provide the necessary voltages. During spin-up, the amplifier is designed to provide up to 750 V to the electrodes, while on the ground up to 1500 V is required.

4.2. Backup control scheme

While it is desired to run the entire mission via the digital control algorithms in the suspension processor, radiation-induced soft failures of the processor which require a full reboot are likely to occur 1–3 times per mission per gyroscope, thus a backup control system is required. In the science mission mode, two separate backup controllers are provided; see Fig. 6. A low control authority controller is provided to take over from the processor during normal operation where only gravity gradient and rotor charge disturbances are in effect. This controller is a simple PD (proportional-derivative) linear controller which will generate specific forces on the rotor up to the order of 10^{-5} m/s^2. While the torque performance of this simple PD controller is worse that baseline digital algorithm, it is tuned so to meet as nearly as possible the science mission control specifications. It is anticipated that the gyroscope can remain in this low backup mode for 1–2 months before adversely affecting the precision of the measurement.

Though the low backup controller is nearly science mission compatible, it is unable to handle the periodic impulsive disturbances caused by micrometeoroid impacts. For this case, and aggressive high authority backup controller is included. This controller aggressively catches and re-centers the gyroscope in the event of a large micrometeoroid impact. It is a bang-bang controller and is constructed to use the full 50 V range of the low noise science drive amplifier. Similarly, the primary digital spin-up controller also has a PD backup control system in the event of a soft computer failure during spin-up.

The selection of which controller operates at any one time is determined by the *control system arbiter*, a simple, robust analog computer in the forward electronics enclosure. This arbiter continuously monitors computer activity as well as the position of the gyroscope. In the event of a computer failure or a gyro excursion out of a pre-determined safety zone, the arbiter autonomously will switch between the prime digital controller, and one of its backup systems. It will return control of the gyroscope to the computer only after it confirms that the computer is operational and functioning properly.

4.3. Spin axis alignment

Though a core goal of the experiment is to minimize disturbance torques on the gyroscope rotor, after initial

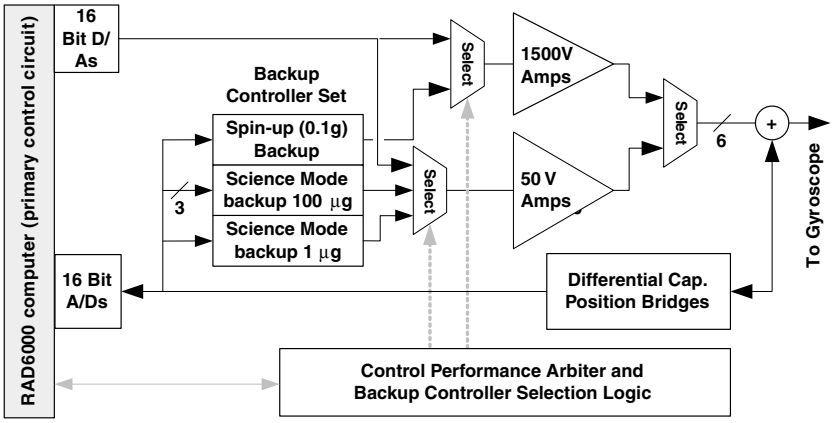

Fig. 6. Block diagram of suspension control system. Primary control path shown by fat line.

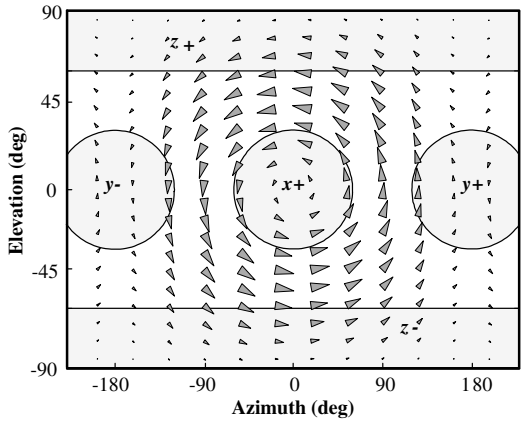

Fig. 7. Torque due to preload electrode voltages on the x-axis causes gyroscope to precess around the same axis.

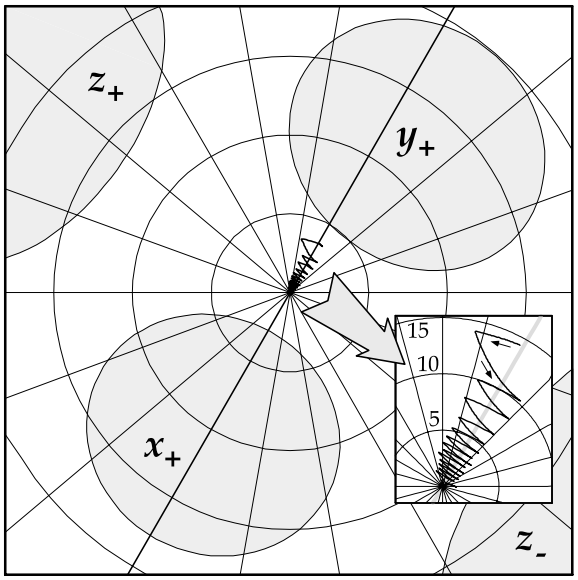

Fig. 8. Spin axis orientation under influence of alternating x- and y-axis dominant preloads (inset shows detail near origin).

spin-up, it is desired to align the spin axis of the rotor to within $1''$ (2.8×10^{-4} deg) of the line of sight of a reference star so to establish the initial conditions for the experiment. As noted in Section 3, the choice of the preload electric fields can either enhance or minimize electrostatic torques on the gyroscope. By judicious choice of preloads in Eq. (7), the net electric field intensity on one axis can be made preferentially larger or smaller than the other axes (while staying consistent with the force constraints given by Eqs. (5) and (6) for each of the three axes). When this electric field imbalance is taken into account in the evaluation of the torque in Eq. (3) along with the fact that the primary non-spherical shape term is the 25 nm centrifugal bulge of the spinning rotor, it is found that the gyroscope will tend to precess around the electrode axis with the largest preload electric field (Bencze, 1997). Fig. 7 shows this effect for the x electrode axis; here the spherical housing is "flattened", showing the x and y electrodes along the equator, with the z pair making up the north and south pole. The arrows indicate the direction and magnitude of the torque on the rotor due to the centrifugal bulge. Though only one electrode axis is shown, the net torque is the superposition of the torques from the axes, and the axis with the largest electric field preload will dominate.

Fig. 8 shows data taken from a test gyroscope with alternating x- and y-axis dominant preloads. Alignment goal is

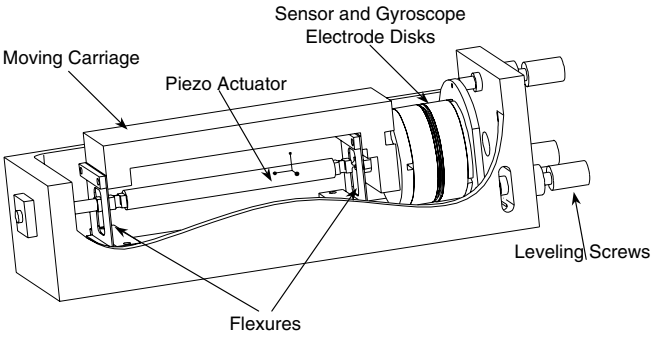

Fig. 9. Schematic view of testbed actuator.

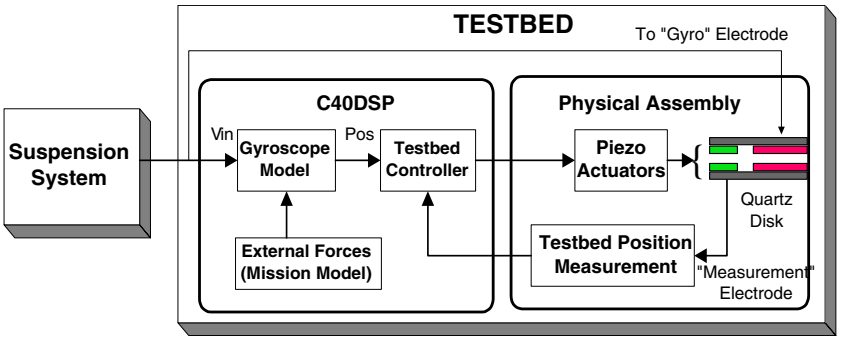

Fig. 10. Schematic view of testbed concept.

the origin. Clearly seen here is the zigzag path of the gyroscope spin axis under the influence of the alternating dominant preloads. While this gyro housing is fixed in the laboratory, the spacecraft will be rolling about an axis through the origin, and a torque rectification scheme has been developed to rectify these torques and thus drive the spin axis to the origin (or other goal orientation) from any initial condition from the spin-up process.

5. Performance verification

A significant problem facing Gravity Probe B is characterizing and verifying the performance of the suspension system levitating the on-orbit gyroscopes without actually having to perform an additional full fledged space experiment. It is necessary to test the closed-loop response of the electrostatic suspension in order to determine the subtleties of the integrated system and to verify compliance with all flight requirements. While the gyroscopes and suspension system are designed with a ground levitation capability needed for functionality checking, the four orders of magnitude separating the ground and on-orbit suspension voltages (1000 V versus 0.1 V) make the ground testing unsuitable for complete verification of on-orbit performance. Computer simulations, with their dependence on idealized models, would provide a less than satisfactory test of the systems.

The solution implemented combines precision engineering with modern control techniques, to create a device with the dynamics of a gyroscope, which operates in a fully defined and controllable environment. The gyroscope 'testbed' consists of six electrode pairs on quartz disks that simulate the six gyroscope electrodes, by generating the required electrode to gyroscope capacitance. Piezoelectric actuators control the spacing between the quartz disk pairs, using the position information supplied by additional measurement electrodes. Complex shielding between the gyroscope and the measurement electrodes on the quartz disks is needed in order to minimize cross talk between the two feedback systems (Brumley, 2003). Fig. 9 shows a schematic view of a complete testbed actuator assembly.

A Texas Instruments 320C40 DSP contains the testbed controller, the gyroscope model, and a science mission model including all on-orbit disturbances, while the suspension system couples directly into the testbed. Fig. 10 shows a representation of the testbed concept. The testbed allows the integrated testing of all functions of the suspension system, including position measurement and control, charge measurement and control, and spin axis alignment using space vehicle roll rate modulation of the suspension voltages. It also allows the testing of all suspension regimes from 1 to 10^{-7} g, while incorporating all on orbit disturbances during both the initial setup and gyroscope spin-up stages, as well as the science mission data acquisition period. The demonstrated position resolution of the testbed is better than 0.1 nm over a bandwidth greater than 300 Hz.

Gravity Probe B is scheduled to be launched on a Boeing Delta II booster from Vandenburg Air Force Base, California, in April, 2004. This work was supported by NASA contract NAS8-39225. Additional information on the Gravity Probe B Relativity Mission can be found at http://einstein.stanford.edu.

References

Turneaure, J.P., et al, The gravity probe B relativity gyroscope experiment: approach to a flight mission, in: Proc. Fourth Marcel Grossmann Meeting on General Relativity (MG4), pp. 411–464, 1996.

Cramer, B. et al. Laser Interferometer Space Antenna, Technology Readiness and Implementation Plan. NASA Jet Propulsion Laboratory, Pasadena, CA, USA, 2003.

Wellstood, F. et al. Integrated DC SQUID magnetometer with high slew rate. Rev. Sci. Instrum. 55 (6), 953–957, 1984.

Smythe, W.R. Static and Dynamic Electricity. McGraw-Hill, New York, 1968.

Eglington, M.L., Authority-on-Demand Adaptive Suspension for the Gravity Probe B Gyroscopes, Doctoral Dissertation, Stanford University, Dept. of Aeronautics and Astronautics, 2000.

Bencze, W.J., Gyroscope Spin Axis Direction Control for the Gravity Probe B Satellite, Doctoral dissertation, Stanford University, Dept. of Electrical Engineering, 1997.

Brumley, R.W., The Testbed Gyroscope Simulator: A Verification of the Gravity Probe B Suspension System, Doctoral Dissertation, Stanford University, Dept. of Electrical Engineering, 2003.